國立交通大學
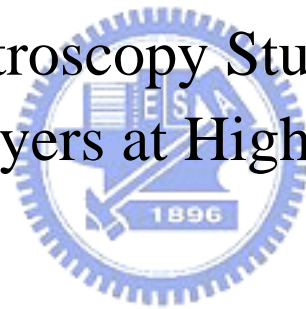# 顯示科技研究所
碩士學位論文

硒化鎘鋅磊晶層的高壓拉曼散射光譜研究

Raman Spectroscopy Study of $Zn_{1-x}Cd_xSe$ Epilayers at High Pressure

研究生：吳聲嵩

指導教授：陳志隆 教授

共同指導教授：周武清 教授

中華民國九十五年七月

硒化鎘鋅磊晶層的高壓拉曼散射光譜研究

Raman Spectroscopy Study of Zn$_{1-x}$Cd$_x$Se Epilayers at High Pressure

研 究 生：吳聲嵩　　　　　　　　Student：Sheng-Sung Wu

指導教授：陳志隆 老師　　　　　　Advisor：Jyh-Long Chern

共同指導教授：周武清 老師　　　　Co-advisor：Wu-Ching Chou

國 立 交 通 大 學

顯 示 科 技 研 究 所

碩 士 論 文

A Thesis
Submitted to Institute of Electronics College of Engineering
National Chiao Tung University
in partial Fulfillment of the Requirements
for the Degree of
Master
in

Display Institute

July 2006

Hsinchu, Taiwan, Republic of China

中華民國九十五年七月

硒化鎘鋅磊晶層的高壓拉曼散射光譜研究

學生：吳聲嵩　　　　　　　　　　指導教授：陳志隆 教授

　　　　　　　　　　　　　　　共同指導教授：周武清 教授

國立交通大學顯示科技研究所

摘　　　　要

　　在本論文中，以微拉曼散射光譜來研究在砷化鎵基板上成長不同鎘含量的硒化鎘鋅磊晶層的光學特性。實驗發現在室溫、大氣壓力下不同鎘含量的硒化鎘鋅磊晶層其縱向光學聲子模頻率和橫向光學聲子模頻率會隨著鎘含量的增加而減少，其強度也有減弱的趨勢。晶格振動模態屬於單模特性。並且利用鑽石高壓砧的技術，在室溫下觀察不同鎘含量樣品的拉曼譜線隨壓力之變化。我們發現在對不同鎘含量的硒化鎘鋅其縱、橫向光學聲子模振動頻率會隨壓力增加而變大，即為有藍位移現象，當壓力加到轉換壓力時，其縱向光學聲子模消失，但橫向光學聲子模仍然存在，此壓力即為半導體由閃鋅礦結構轉變為岩鹽結構的臨界壓力。我們發現硒化鎘鋅磊晶層之相位轉變壓力會隨著鎘含量的增加而減少，此現象歸諸為鎘含量增加而造成的晶格不穩定。最後我們也計算聲子頻率與 Grünesien 參數隨壓力變化的關係。

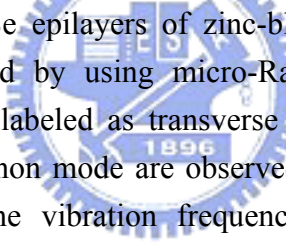# Raman Spectroscopy Study of $Zn_{1-x}Cd_xSe$ Epilayers at High Pressure

Student：Sheng-Sung Wu   Advisor：Prof. Jyh-Long Chern

Co-advisor：Prof. Wu-Ching Chou

Display Institute
National Chiao Tung University

ABSTRACT

In this thesis, $Zn_{1-x}Cd_xSe$ epilayers of zinc-blende phase were grown on the GaAs substrates were studied by using micro-Raman scattering experiment. At ambient pressure, two peaks labeled as transverse optical (TO) phonon mode and longitudinal optical (LO) phonon mode are observed for each $Zn_{1-x}Cd_xSe$ epilayers. From the Raman spectra, the vibration frequency decreases and the linewidth increases with the Cd concentration. The lattice vibration mode behavior of $Zn_{1-x}Cd_xSe$ epilayers belongs to the one-mode behavior. The high pressures were generated by using a diamond anvil cell. For $Zn_{1-x}Cd_xSe$ epilayers with $x = 0.00$, 0.06, 0.08, 0.14, 0.25, and 0.32, all Raman peaks blue shifted to higher frequencies when the pressure was increased. As the pressure was increased to the transition pressure, the LO phonon disappeared. The disappearance of the LO phonon in Raman spectra at high pressure is attributed to the semiconductor to metal phase transition. The metallization occurred when the crystal structure transformed from a four-coordinated zinc-blende (ZB) phase into a six-coordinated rock-salt (RS) phase. As x was increased, the semiconductor to metal-transition pressure decreased. The decrease in transition pressure with x implies the decreasing crystal stability with x. Finally, we also calculated the pressure variation of the phonon frequencies and Grünesien parameters of the two optical modes.

ACKNOWLEDGEMENT

CONTENTS

LIST OF FIGURES

LIST OF TABLES

Chapter 1

Introduction

The wide band gap II-VI compound semiconductor family has attracted intense interest for the past decades due to its applications in optoelectronic devices. In particularly, ZnSe-based ternary compound semiconductors, such as $Zn_{1-x}Cd_xSe$, $Zn_{1-x}Mn_xSe$, have attracted much attention due to its tunability in lattice constant and band gap. Among them, $Zn_{1-x}Cd_xSe$ is one of the most intenerating compounds because its band gap covers most of visible light region from blue to red. Ternary compound $Zn_{1-x}Cd_xSe$ was widely used as an active layer in a strained single $Zn_{1-x}Cd_xSe$ quantum well with ZnSSe or ZnSe barrier of the II-VI semiconductor blue-green diode lasers [1, 2, 3]. As a result, the optical and electrical properties of $Zn_{1-x}Cd_xSe$ epilayers grown by molecular beam epitaxy (MBE) were studied extensively.

In past decades, several kinds of high pressure studies on III-V and II-VI semiconductors have been performed. Ves et al. investigated the band shift of ZnSe as a function of pressure by transmission experiment [4]. The structure transition from zinc-blende to rock-salt phase was identified by optical absorption experiment. The x-ray diffraction experiments were carried out to observe the structure transformations at high pressure by McMahon et al. [5] and Greene et al. [6]. The resistance measurement revealed metallization process at high pressure of semiconductor [7]. Usually, the semiconductor-metal transition pressure can be identified by the energy-dispersive x-ray diffraction (EDXD) which measures change of crystal structure. It accompanies disappearance of the longitudinal optical (LO) phonon mode in Raman spectra [8]. Hence, the Raman scattering studies under hydrostatic pressure

is a powerful tool to investigate the phase transition of crystal structure of semiconductor materials.

Raman scattering studies at high pressure for III-V and II-VI semiconductors have received much attention in recent year [9, 10, 11]. Recently, the Raman scattering experiments were applied to study the pressure effect on $Zn_{1-x}Fe_xSe$ [8], $Zn_{1-x}Co_xSe$ [12], and $Zn_{1-x}Mn_xSe$ [13, 14] crystals. To our knowledge, study of $Zn_{1-x}Cd_xSe$ epilayers of zinc-blende phase grown by molecular beam epitaxy is rare. In this thesis, the Raman scattering of $Zn_{1-x}Cd_xSe$ epilayers at room temperature and under hydrostatic pressure reported.

In Chapter 2, the experimental details of highpressure Raman scattering were described. The experimental results of the lattice vibration of $Zn_{1-x}Cd_xSe$ epilayers at high pressure were presented in Chapter 3. Finally, Chapter 4 concludes our experimental results and gives future direction.
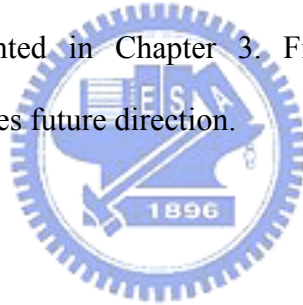
Chapter 2

Principle of Experiment

In this chapter, we describe the experimental techniques used in this thesis. The experimental techniques include high-pressure technique, and micro-Raman scattering measurement. The sample preparation which was used in the high-pressure experiment is also presented.

2.1 Preparation of Sample

In this work, the $Zn_{1-x}Cd_xSe$ epilayers of zinc-blende phase were grown on the (001) GaAs substrates using the Veeco Applied EPI 620 molecular beam epitaxy system. The GaAs substrate was mounted on molybdenum disk holder by Indium. After the substrate holder was loaded on the transfer rod in the introduction chamber. We turned on the oil free diaphragm pump and the turbo pump. When the introduction chamber's pressure is below 10^{-8} torr, we open the manual gate valve and transfer the substrate holder (molybdenum disk) to the growth chamber by the substrate transfer arm. The substrate temperature was raised up to 650 ^{o}C for removing the oxide on the GaAs substrate. After clear RHEED pattern was observed, the substrate temperature was decreased to 300 ^{o}C for growing the $Zn_{1-x}Cd_xSe$ epilayers. For the $Zn_{1-x}Cd_xSe$ epilayers, the cell temperatures of Zn and Cd were ranged from 300 ^{o}C to 260 ^{o}C and from 230 ^{o}C to 210 ^{o}C, respectively. While, the cell temperature of Se was fixed at 175 ^{o}C. The substrate temperatures were set at 300 ^{o}C. Under the above growth conditions, the growth rate of 0.35 Å/s was obtained. The structures of $Zn_{1-x}Cd_xSe$ epilayers were plot in Fig. 2.1. The sample thickness of $Zn_{1-x}Cd_xSe$ epilayers was fixed to be about

0.5 μm. The growth parameters of the $Zn_{1-x}Cd_xSe$ epilayers were shown in Table 2-1.

2.2 High-pressure Technique

2.2-1 Diamond Anvil Cell

The diamond anvil cell (DAC) was first developed by Jamieson, Lawson, and Nachtrieb in 1959. The components of the diamond anvil cell are shown in Fig. 2.2. In our experiment, the pressure was generated by using diamond anvil cell. The principle of all high-pressure cells, is similar; a force F is applied to a small surface of area S, creating a pressure $P = F / S$, which can be made large by reducing the size of the area of contact. The basic operating principle of the DAC is very simple. A sample placed between the flat parallel faces of two opposed diamond anvil is subjected to pressure when a force pushes the two opposed anvils together.

In the DAC, the sample is placed between the flat faces (culets) of two brilliant-cut diamonds. The culets are separated by a thin metallic foil (gasket) which has previously been indented zone. There is a small hole constituting the pressure chamber into which the sample is placed. The selection of diamonds and size depend upon the type of DAC and the nature of investigation. Typical dimensions are 0.3-0.7 mm for the diameter of the culet, 0.3-0.2 mm for the thickness of the gasket, and about 50-100 μm for the diameter of the circular hole. The sample is normally immersed in a fluid, which fills the chamber and acts as a pressure medium ensuring hydrostatic and homogeneous conditions.

In the Fig. 2.2, A is the hemisphere rockers on which the diamond anvil was mounted; B are two diamonds; C is a gasket. A spring lever-arm A is employed to generate force on the diamond surfaces. Force is applied through the lever-arm, when

the Bellville spring washers are compressed by the turn of the screw, making the two opposed diamonds pressing mutually. Then, we can generate a uniform and continuously pressure as the screw is rotated.

2.2-2 Pressure Medium

In order to generate a hydrostatic pressure environment for samples, a fluid pressure medium is required. Various fluids have been used, but a 4 : 1 methanol-ethanol mixture has been proved to be very popular. Unfortunately, the use of fluids is valid only to about 10 GPa, since most liquids become solids above this pressure. Deionized -water is also considered to be a pressure medium, but it transfers to solid ice VI and ice VII at 0.6 and 2.1 GPa, respectively.

However, previous study shown that the R1-R2 splitting in the ruby fluorescence was maintained well up to 16.7 GPa, therefore, the non-hydrostatic components of water is not a serious problem below 16.7 GPa [15]. In the present study, such a splitting was well recorded up to 25.4 GPa as shown in Fig. 2.3. Hence, deionized -water seems to be a suitable pressure medium in the high pressure study. For the reason we choose deionized -water pressure medium in our experiments.

2.2-3 Pressure Calibration

Various methods of pressure calibration involving the DAC have been used. Pressure in the DAC was estimated by calculating force over area, the known fixed point, and in high-pressure X-ray studies by internal markers such as NaCl or silver. However, these methods are not convenient and are often proved to be inaccurate.

With the introduction of the ruby fluorescence method in 1972 by Foreman et al. [16] a major obstacle with the DAC, namely, pressure calibration, was removed,

clearing the way for widespread use of the DAC for high-pressure physical investigation. Foreman et al. first showed the R-line on Cr^{+3}-doped Al_2O_3 shift linearly with hydrostatic pressure in the range of 0.1-2.2 GPa, and that the R-line broadens if the ruby experiences non-hydrostatic stresses. A tiny ruby chip of 5-10 μm in the pressure medium along with the sample, and the fluorescence of the ruby chip is excited by either a Ar^{+2} laser line or any source of strong light. Fig. 2.4 shows the energy levels and the resulting absorption and luminescence for Cr^{+3} ions in ruby [17].

Piermarinal et al. [18] calibrated the R-line to 19.5 GPa against the compression of NaCl by using Decker equation of state for NaCl. The R-lines of ruby are intense, and the doublet R1 and R2 have the delta wavelength 964.2 and 692.7 nm, respectively, at atmospheric pressure. At high pressure these shifts to higher wavelength and the shift is measured linearly with increasing pressure.

2.3 Micro-Raman Scattering Experiments

2.3-1 The Principle of Raman Scattering

All the Raman parameters – band frequencies and intensity, line shape and linewidth, polarization behavior – can be used to characterize the lattice, impurities, and free carriers in a semiconductor. The intensity gives information about crystallinity. The linewidths increase when a material is damaged or disordered, because these conditions increase the phonon damping or break the momentum conservation during the Raman scattering process. The strengths and frequencies of the phonons can be used to determine the degree of alloying in a ternary material [19].

Raman scattering involves a change in photon frequency. When light

encounters the surface of a semiconductor, the following situations can usually occur: for example, reflected, transmitted, absorbed, or Rayleigh scattered. In these situations, there are no change in photon frequency. However, a small fraction of light may interacts elastically with phonon modes, producing outgoing photons whose frequencies are shifted from the incoming ones. These are the Raman-scattered photons. The interaction of the incident light with optical phonons is called Raman scattering. When the polarization of optical phonon is transverse (longitudinal) relative to their wavevector of photon, it is call TO (LO) mode. Photon gains energy by absorbing a phonon (anti-Stokes shifted), or loses energy by emitting one (Stokes shifted). The law of conservation energy and momentum must be applied in the process. The conservation conditions are

$$h v_s = h v_i \pm h v_0 , \tag{2.1}$$

$$k_s = k_i \pm k_0 , \tag{2.2}$$

Where the subscript "s" in the formula stands for scattering: "i" stands for incident and "0" stands for optical phonon. The puls sign stands fot anti-Stokes shift and minus sign is stands for Stokes shift. Normally, the intensity of the anti-Stokes modes is much weaker than that of the Stokes components, because usually these are few phonons to be absorbed compared to the density of phonons that can be emitted. Raman scattering is inherently a weak process, but lasers provide enough power such that the spectra can be routinely measured [20].

2.3-2 Experimental Setup

The schematic diagram of the Raman scattering experiment is shown in Fig. 2.5. In this work, the Raman scattering measurements were performed by a Jobin-Yvon micro-Raman system. The Raman spectra at room temperature were excited by using

the 514.5 nm line from an argon-ion laser. Usually, a laser beam with a power of 90 mW was focused to a size of about 2 μm on the sample surface in the DAC. To exclude the Reyleigh scattering, we used notch filter to filter out the Reyleigh scattering of the laser. The intensity of Raman lines were normalized to the power of the laser as measure by a power meter and the backscattering Raman signals were collected by the SPEX 1404 double-grating spectrometer and detected by a LN_2 cooled charge coupled device (CCD). The spectrometer was controlled by a computer, which was used to store and plot the collected data.

2.4 Experimental Process

The $Zn_{1-x}Cd_xSe$ epilayers grown by MBE were ground into thin films with the thickness of 100 μm the followed by chemical etching using NaOH mixed with H_2O_2 and deionized-water to remove the GaAs substrate. To obtain high pressure up to about 20 GPa, the $Zn_{1-x}Cd_xSe$ epilayers and ruby chip (about 1 μm in size) were sealed with the pressure transmitting medium (deionized-water) in the sample chamber which was a hole of 170 μm diameter and 100 μm thick drilled on gasket which has an original thickness of 250 μm. The epilayers without GaAs substrates were loaded along with ruby powder into a diamond anvil cell. The pressure determination was done by reading the peak position of the ruby R1 fluorescence line.

Table 2-1   Growth condition of $Zn_{1-x}Cd_xSe$ epilayers.

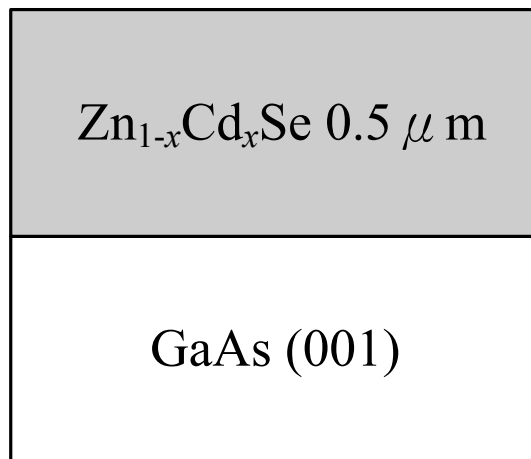| Sample number	substrate (°C)	Zn (°C)	Se (°C)	Cd (°C)	x
1	300	300	175	—	0.00
2	300	300	175	200	0.06
3	300	300	175	210	0.08
4	300	300	175	225	0.14
5	300	295	175	230	0.25
6	300	290	175	230	0.32

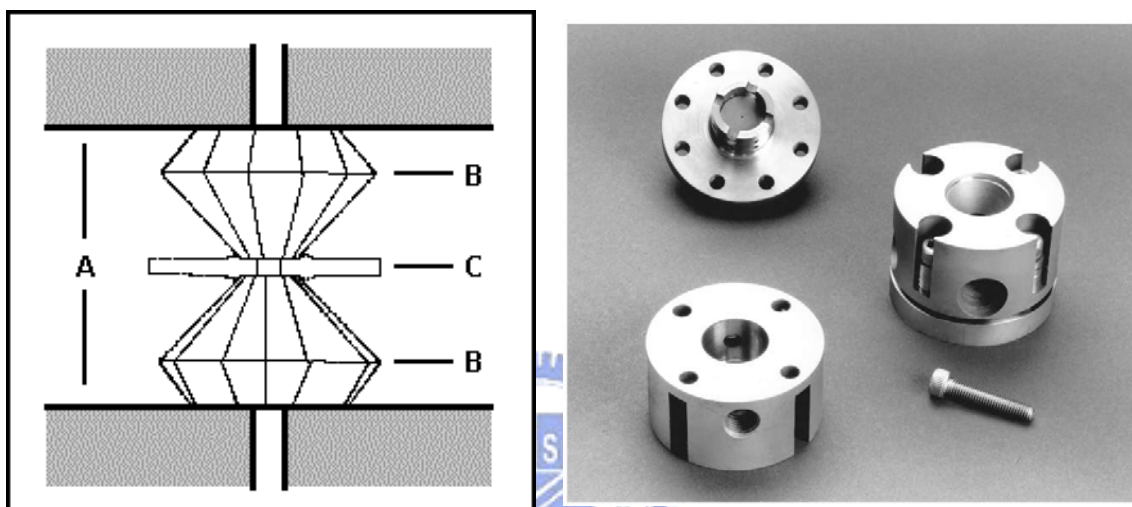Fig. 2.1   Schematic structure for $Zn_{1-x}Cd_xSe$ epilayers.

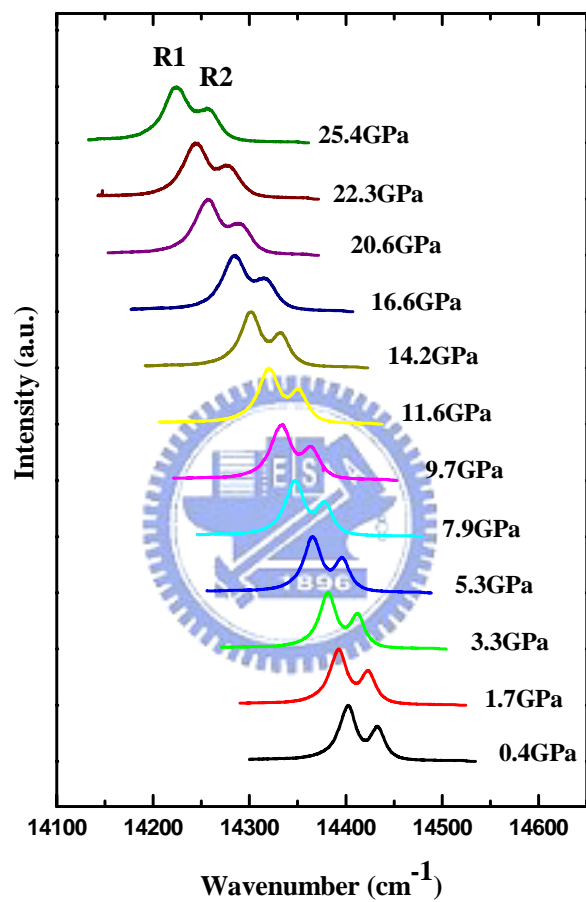Fig. 2.2   Basic setup of diamond anvil cell.

Fig. 2.3 Ruby fluorescence verse pressure in a pressure medium of deionized-water. The right -hand and left -hand side peaks of the plots present R1 and R2 peaks of the ruby fluorescence lines, respectively.
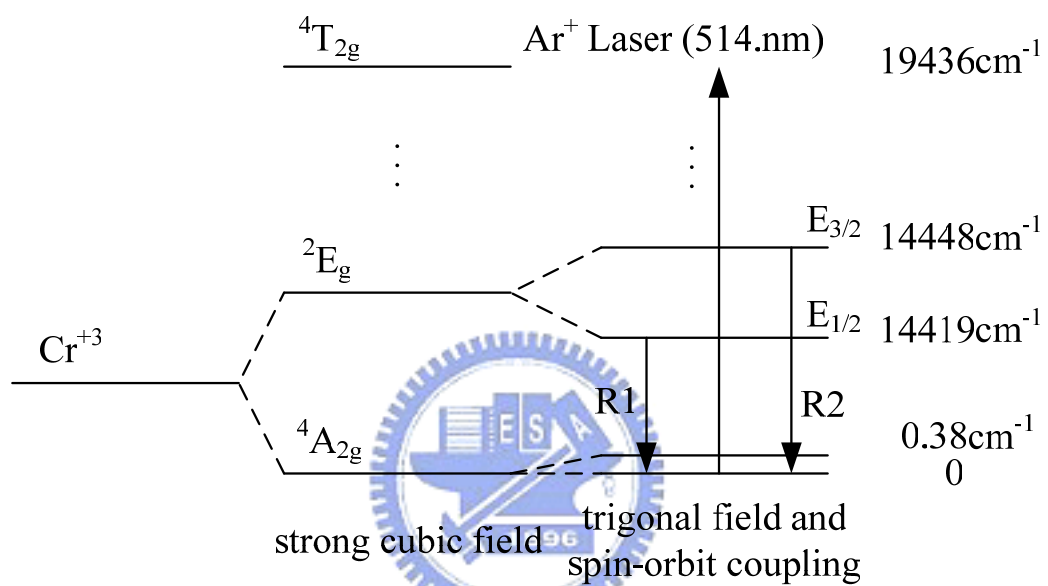
Fig. 2.4   Energy level of Cr^{+3} in Al_2O_3. The transitions of $E_{1/2}{\to}A$ and $E_{3/2}{\to}A$ give rise to R1 and R2 lines, respectively.
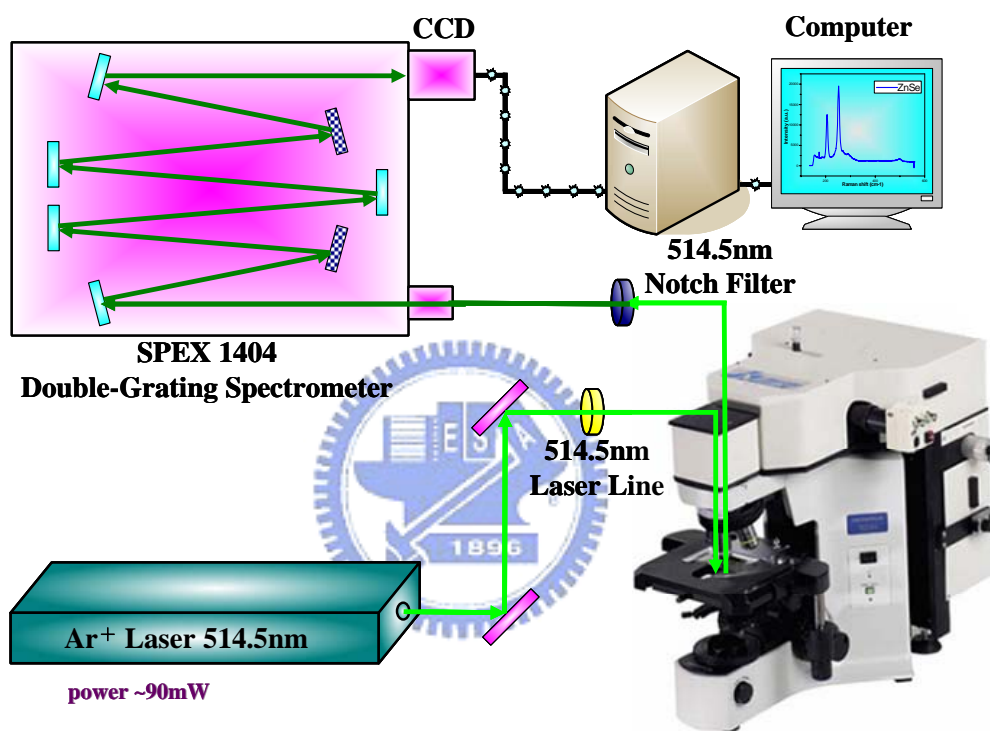
Fig. 2.5 Schematic diagram of Raman scattering experiment.

Chapter 3
Result and Discussion

3.1 Raman Scattering of $Zn_{1-x}Cd_xSe$ Epilayers at Atomspheric Pressure

We have measured the phonon frequencies of the $Zn_{1-x}Cd_xSe$ epilayers at room temperature and various pressures by Raman scattering system. In the backscattering geometry used in our experiment, the LO phonon mode is allowed while the TO phonon mode is forbidden. For the Raman scattering experiment, the GaAs substrate were removed by mechanical polishing. At atmospheric pressure, two peaks labeled as TO phonon mode and LO phonon mode are observed for each $Zn_{1-x}Cd_xSe$ epilayer in Fig. 3.1. For $x = 0.00$, the TO and LO are observed at 205.3 cm^{-1} and 252.1 cm^{-1}, respectively. For $x = 0.06$, the TO and LO are observed at 203.1 cm^{-1} and 248.5 cm^{-1}, respectively. For $x = 0.08$, the TO and LO are observed at 201.4 cm^{-1} and 246.6 cm^{-1}, respectively. We only observe one peak labeled as LO for $x = 0.14$, $x = 0.25$, and $x = 0.32$ at atmospheric pressure. The LO are observed at 241.3 cm^{-1}, 241.3 cm^{-1}, and 240.2 cm^{-1}, respectively. The variation of these phonon frequencies with Cd concentration fraction x is shown in Fig. 3.2. In this figure, phonon frequencies of CdSe obtained from other reference are also shown by open circle and open square [21]. From this figure, Raman measurements on samples of MBE grown $Zn_{1-x}Cd_xSe$ epilayers show a linear variation of frequencies with the Cd concentration fraction x. The Raman peaks of $Zn_{1-x}Cd_xSe$ epilayers decrease frequency and increase linewidth with the increasing Cd concentration. It implies the softening of the lattice. This agrees with the observation that the high Cd concentration increases alloy potential

fluctuation [1]. With increasing Cd concentration, the phonon vibration mode has a redshift, and the mode intensity weakens. The fact that the atomic radius of Cd is greater than Zn leads to the increase in lattice constant. As a result, the frequencies of the quasi-harmonic vibration of the crystal should be decreased. As shown in this figure, the results of our experiments reveal that $Zn_{1-x}Cd_xSe$ is a one-mode system. Whether a mixed crystal system $A_{1-x}B_xC$ will exhibit one-, two-, and mixed-mode behavior type depends almost entirely on the relative masses of the atoms A, B, and C. In the one-mode behavior, the zone-center optical phonon frequencies vary continuously with concentration within the frequencies of the two end members. In two-mode behavior, each TO-LO phonon pair for an end members degenerates to an impurity mode of the other end member. Between these limits lies the mixed-mode, which shows intermediate behaviors. Based on this consideration, Chang and Mitra have derived a criterion in order to determine the one-, two-, or mixed-mode behavior type [22]. The criterion for one mode behavior is $m_A > \mu_{BC}$ i.e. for one-mode mixed crystal, the mass of one substituting element is smaller than the reduced mass of the compound formed by the other elements, at both ends of its composition range [23]. If this is violated the alloy will exhibit two-mode behavior. In our considerations, the masses of each component are chosen as follows: $m_{Zn} = 65.38$ amu., $m_{Cd} = 112.41$ amu., and $m_{Se} = 78.96$ amu.. For $Zn_{1-x}Cd_xSe$, the mass of Cd is greater than the reduced mass of ZnSe, and the mass of Zn is greater than the reduced mass of CdSe. As a result, $Zn_{1-x}Cd_xSe$ epilayers exhibits one-mode behavior for all values of x between 0 and 1. It is in agreement with our experimental results. However, there is some controversy in the literature. Alonso et al. performed Raman measurements on $Zn_{1-x}Cd_xSe$ in the whole compositional range [21]. They found $Zn_{1-x}Cd_xSe$ exhibites a mixed-mode behavior. J. Camacho et al. also found a mixed-mode behavior in

$Zn_{1-x}Cd_xSe$ [24]. However, more recent Raman measurements seem to support that $Zn_{1-x}Cd_xSe$ has a one-mode behavior [23, 25, 26].

3.2 Raman Scattering of $Zn_{1-x}Cd_xSe$ Epilayers at High Presssure

For the high-pressure Raman scattering experiments, high pressures were generated by using the diamond anvil cell. When the pressure is increased, the force acted on the crystal becomes larger and this force will compress the whole volume of the crystal. Therefore the distances among atoms would accordingly decrease. When atoms become closer to each other, the repulsion force induced by outer-shell electrons of neighboring atoms becomes larger and larger. And this makes the whole crystal unstable. As a result, the whole crystal structure would change to a more stable crystal structure. The structure change could induce energy shift of phonon, and it can be studied by Raman scattering. The Raman spectroscopy of $Zn_{1-x}Cd_xSe$ epilayers for x = 0.00, 0.06, 0.08, 0.14, 0.25, and 0.32 at various pressures and room temperature are shown in Fig. 3.3-3.8. In Fig. 3.3-3.8, intensities of all these Raman modes decrease as the pressure is increased. According to Fig. 3.3-3.8, we find that the LO phonon modes disappeared and the TO phonon modes broaden at different pressure. For x = 0.00, the LO phonon mode disappeared and TO phonon mode broadened at 12.9 GPa. For x = 0.06, the LO phonon mode disappeared and TO phonon mode broadened at 12.3 GPa. For x = 0.08, the LO phonon mode disappeared and TO phonon mode broadened at 11.4 GPa. For x = 0.14, the LO phonon mode is disappeared and TO phonon mode broadened at 7.1 GPa. For x = 0.25, the LO phonon mode disappeared and TO phonon mode broadened at 10.0 GPa. For x = 0.32, the LO phonon mode disappeared and TO phonon mode broadened at 9.5 GPa. Usually, the semiconductor-metal transition

pressure was identified by the energy-dispersive x-ray diffraction (EDXD) result which corresponds to a change of the crystal structure and accompanies the disappearance of the LO phonon mode [8]. As x is increased, the semiconductor to metal-transition pressure decreased. However, we have found the transition pressure increased when Cd concentration x is increased from 0.14 to 0.25. The transition pressures of the $Zn_{1-x}Cd_xSe$ epilayers for x up to 0.32 are plotted in Fig. 3.15. The decrease in transition pressure with x implies the decreasing crystal stability with x. However, the reason of the increase in transition pressure is unidentified.

The variation of Raman shift of LO and TO for ZnSe, $Zn_{0.94}Cd_{0.06}Se$, $Zn_{0.92}Cd_{0.08}Se$, $Zn_{0.86}Cd_{0.14}Se$, $Zn_{0.75}Cd_{0.25}Se$, and $Zn_{0.68}Cd_{0.32}Se$ epilayers as a function of pressure are shown in Fig. 3.9-3.14, respectively. The circles and squares represents for TO mode and LO mode, respectively. The lines are quadratic polynomial fitting lines that conclude the behavior of each Raman modes with increasing pressure. From these figures, one can clearly see the variation of different Raman modes at different pressures.

It is clear that for $Zn_{1-x}Cd_xSe$ epilayers with x = 0.00, 0.06, 0.08, 0.14, 0.25, and 0.32, all Raman modes blue shift to higher frequencies when the pressure increases. The relationship of these Raman mode frequencies versus pressure of ZnSe, $Zn_{0.94}Cd_{0.06}Se$, $Zn_{0.92}Cd_{0.08}Se$, $Zn_{0.86}Cd_{0.14}Se$, $Zn_{0.75}Cd_{0.25}Se$, and $Zn_{0.68}Cd_{0.32}Se$ epilayers can be obtained by the quadratic polynomial fitting and are plotted as the solid curve, in Fig. 3.9-3.14, respectively. The solid symbols shown in the figures are the results of our experimental data. The quadratic polynomial fitting formulas for ZnSe are expressed as follows:

$$\omega_{LO} = 252.1 + 3.28P - 0.041P^2 \tag{3.1}$$

$$\omega_{TO} = 205.3 + 4.66P - 0.090P^2 \tag{3.2},$$

for $Zn_{0.94}Cd_{0.06}Se$ are expressed as follows:

$$\omega_{LO} = 248.7 + 4.73P - 0.165P^2 \quad\quad (3.3)$$

$$\omega_{TO} = 203.3 + 4.88P - 0.071P^2 \quad\quad (3.4),$$

for $Zn_{0.92}Cd_{0.08}Se$ are expressed as follows:

$$\omega_{LO} = 246.2 + 3.50P - 0.008P^2 \quad\quad (3.5)$$

$$\omega_{TO} = 205.3 + 3.95P - 0.071P^2 \quad\quad (3.6),$$

for $Zn_{0.86}Cd_{0.14}Se$ is expressed as follows:

$$\omega_{LO} = 243.2 + 2.55P - 0.208P^2 \quad\quad (3.7),$$

for $Zn_{0.75}Cd_{0.25}Se$ is expressed as follows:

$$\omega_{LO} = 241.5 + 3.73P - 0.041P^2 \quad\quad (3.8),$$

similarly, for $Zn_{0.68}Cd_{0.32}Se$, the fitting formulas can be expressed as follows:

$$\omega_{LO} = 239.2 + 4.92P - 0.162P^2 \quad\quad (3.9),$$

where ω is the wavenumber in cm^{-1} and P is the pressure in GPa.

In general, the crystal ionicity can be expressed by the Grünesien parameters, which can be calculated from the pressure shifts of the LO and TO phonons of $Zn_{1-x}Cd_xSe$ measured by the micro-Raman scattering experiments. The Grünesien parameter γ_i for a quasi-harmonic mode i of frequency ω_i is defined by [27]

$$\gamma_i = -\frac{\partial \ln \omega_i}{\partial \ln v} = \frac{1}{\beta}\frac{\partial \ln \omega_i}{\partial p} = \frac{k_0}{\omega_i}\frac{d\omega_i}{dp} \quad\quad (3.10),$$

where β is the isothermal volume compressibility; v is the molar volume in cm^3/mol; k_0 is the bulk modulus for $Zn_{1-x}Cd_xSe$. The bulk modulus of $Zn_{1-x}Cd_xSe$ is unknown, but the values of k_{0ZnSe}=65.6 GPa [28] and k_{0CdSe}=54.6 GPa [29]. In our samples, Cd concentration x is low. Hence, $k_{0Zn_{1-x}Cd_xSe}$ was taken as 65.6 GPa from the

value of ZnSe at zero pressure. The pressure effect on Raman vibration modes of Zn$_{1-x}$Cd$_x$Se at room temperature are shown in Table 3-1. As a comparison with previous works [30], we found $\gamma_{TO} > \gamma_{LO}$ for all Zn$_{1-x}$Cd$_x$Se epilayers. This indicates that as the crystal is compressed, there is a decrease in the ratio of LO and TO mode frequencies. Further, the calculated $\gamma_{TO} / \gamma_{LO}$ for ZnSe, Zn$_{0.94}$Cd$_{0.06}$Se, and Zn$_{0.92}$Cd$_{0.08}$Se are 1.752, 1.256, and 1.298, respectively. This manifests that ZnSe has a higher ionicity than Zn$_{0.94}$Cd$_{0.06}$Se and Zn$_{0.92}$Cd$_{0.08}$Se.

We may use a spring model to explain why Raman modes blue shift to higher frequencies with increasing pressure. As mentioned before, the interaction force between any two neighboring atoms in a crystal can be considered as having a spring connecting to each other. The force constant of this spring will be different depending on the strength of chemical bonding between atoms. We may consider the force constants between atoms become larger as the pressure was increase. As a result, the phonon vibration energy increases as the pressure is increased.
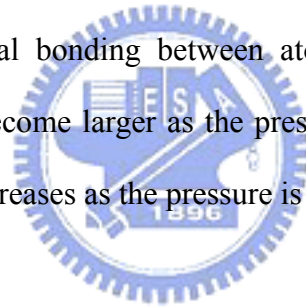
Table 3-1   Effect of pressure on various Raman vibrational modes of $Zn_{1-x}Cd_xSe$ at room temperature. The value of mode frequencies ω_i, pressure dependence $\dfrac{d\omega_i}{dp}$, and mode Grünesien parameter γ_i were obtained at ambient condition.

| Sample	mode	fitting equation	ω_i cm^{-1}	$d\omega_i/dp$ cm^{-1}/GPa	γ_i	$d\gamma_i/dp$ 1/GPa
ZnSe	LO	$252.1+3.28P-0.041P^2$	252.1	$3.28-0.082P$	0.85	$-0.03+1.12\times10^{-3}P$
	TO	$205.3+4.66P-0.090P^2$	205.3	$4.66-0.180P$	1.49	$-0.06+5.18\times10^{-3}P$
$Zn_{0.94}Cd_{0.06}Se$	LO	$248.7+4.73P-0.165P^2$	248.7	$4.73-0.330P$	1.25	$-0.09+5.58\times10^{-3}P$
	TO	$203.3+4.88P-0.071P^2$	203.3	$4.88-0.142P$	1.57	$-0.08+4.86\times10^{-4}P$
$Zn_{0.92}Cd_{0.08}Se$	LO	$246.0+3.63P-0.008P^2$	246.0	$3.63-0.016P$	0.97	$-0.01+8.66\times10^{-4}P$
	TO	$205.3+3.95P+0.071P^2$	205.3	$3.95+0.142P$	1.26	$0.02-1.67\times10^{-3}P$
$Zn_{0.86}Cd_{0.14}Se$	LO	$243.2+2.55P+0.208P^2$	243.2	$2.55+0.416P$	0.69	$0.10+3.37\times10^{-3}P$
$Zn_{0.75}Cd_{0.25}Se$	LO	$241.5+3.73P-0.041P^2$	241.5	$3.73-0.082P$	1.01	$-0.04+1.44\times10^{-3}P$
$Zn_{0.68}Cd_{0.32}Se$	LO	$239.2+4.92P-0.162P^2$	239.2	$4.92-0.324P$	1.34	$-0.11+6.30\times10^{-3}P$
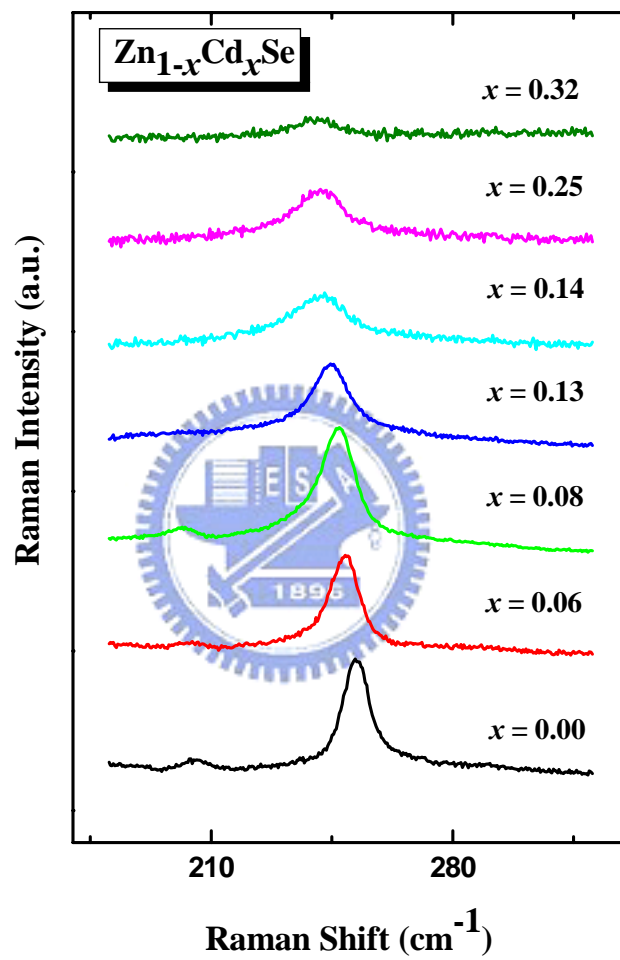
Fig. 3.1 Raman spectra of $Zn_{1-x}Cd_xSe$ for x = 0.00, 0.06, 0.08, 0.13, 0.14, 0.25, and 0.32 at ambient pressure.
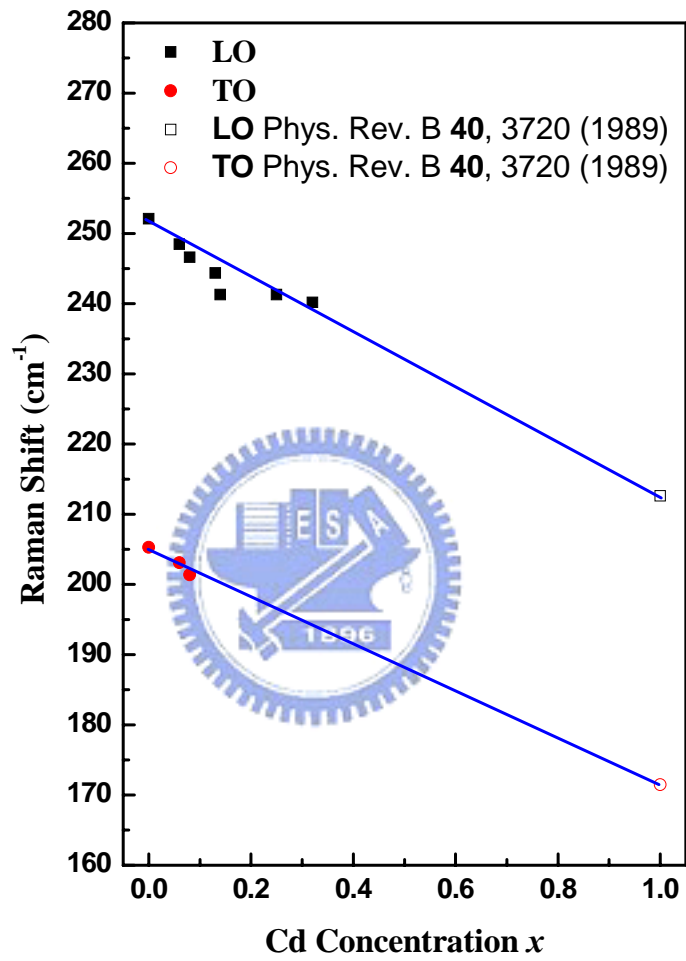
Fig. 3.2　Composition dependence of the zone-center optical phonon frequencies
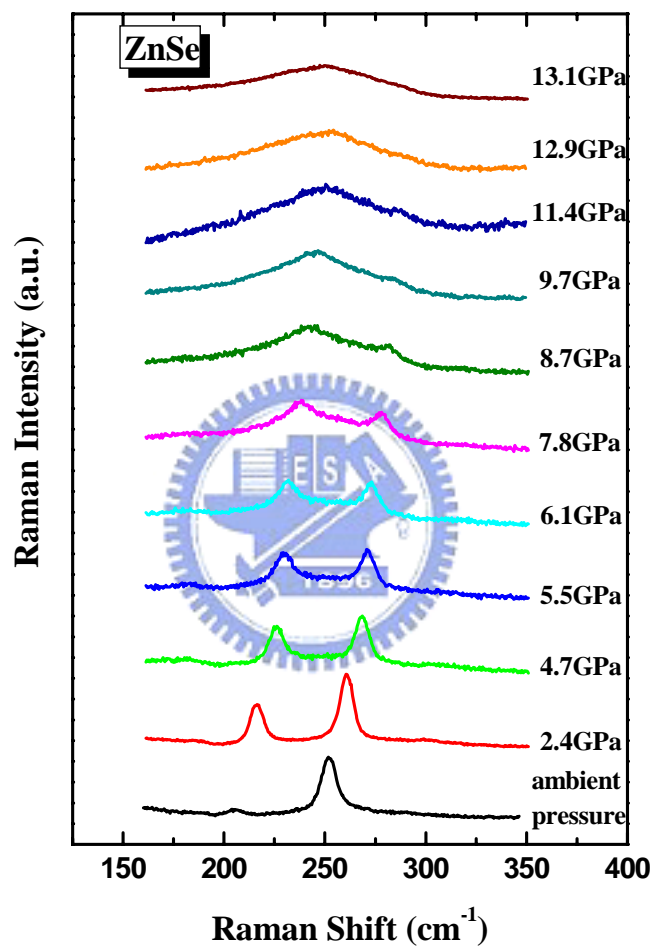
in zinc-blende $Zn_{1-x}Cd_xSe$.

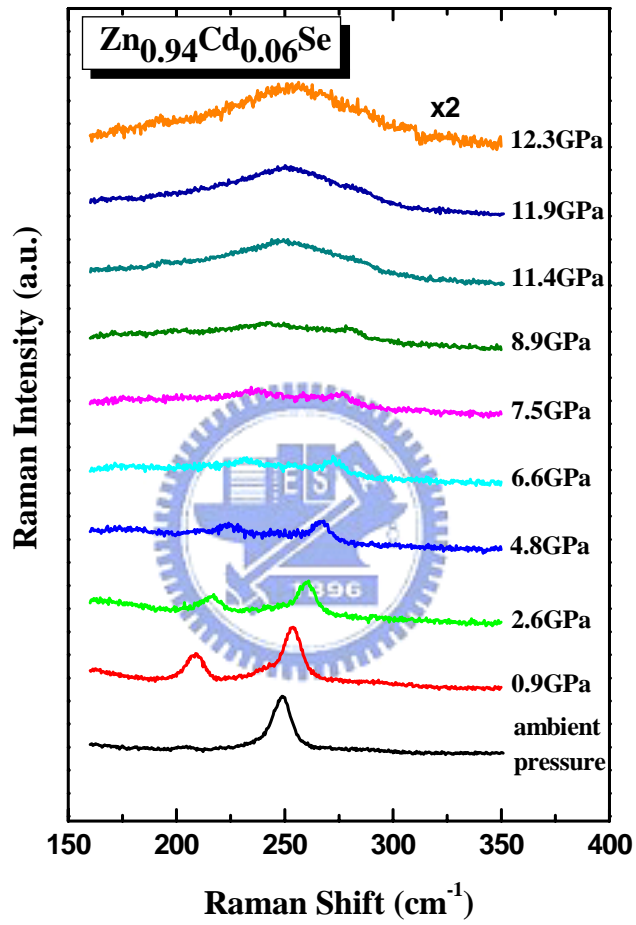Fig. 3.3   Raman spectra of ZnSe at different pressure.

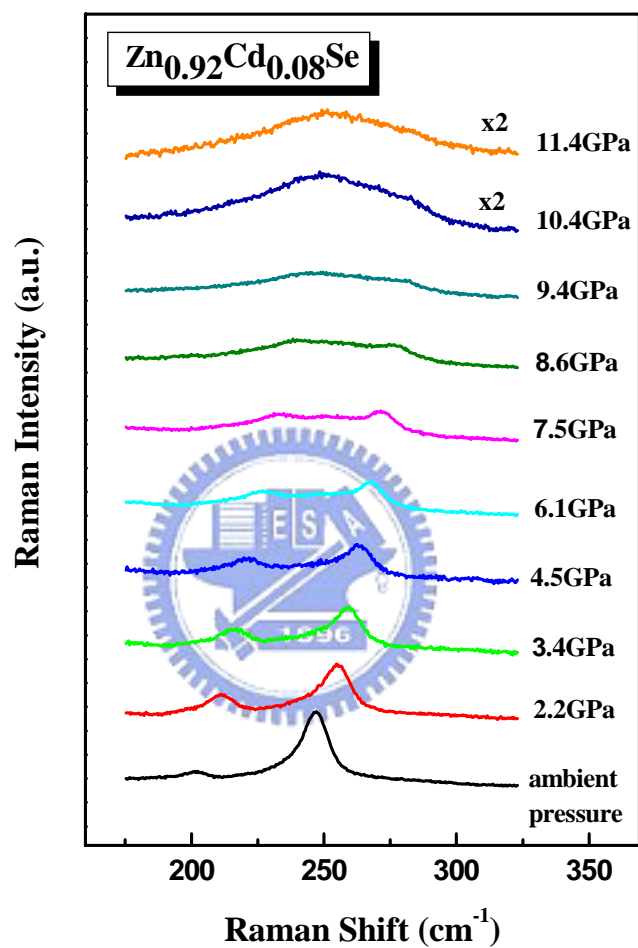Fig. 3.4   Raman spectra of $Zn_{0.94}Cd_{0.06}Se$ at different pressure.

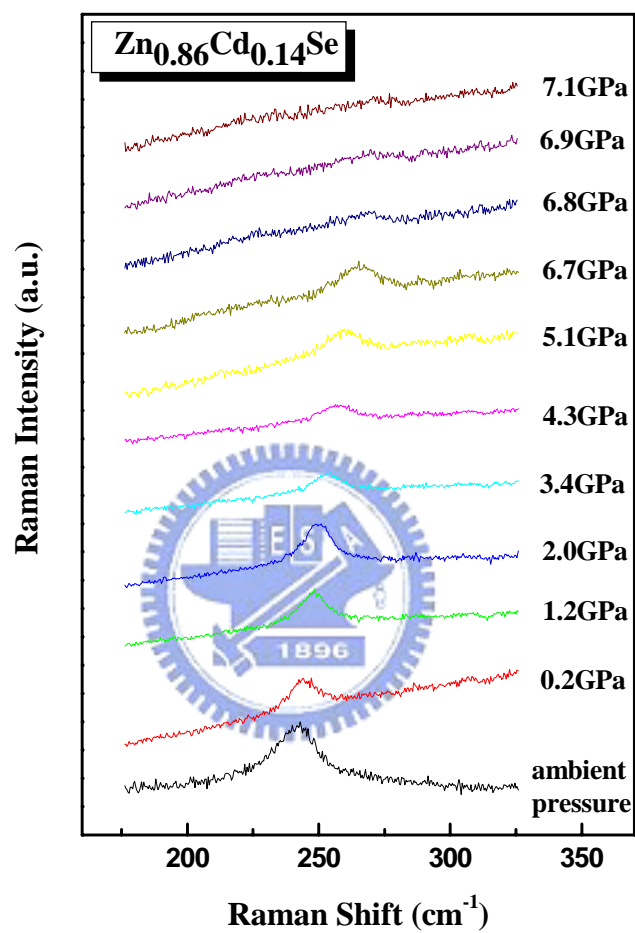Fig. 3.5 Raman spectra of $Zn_{0.92}Cd_{0.08}Se$ at different pressure.

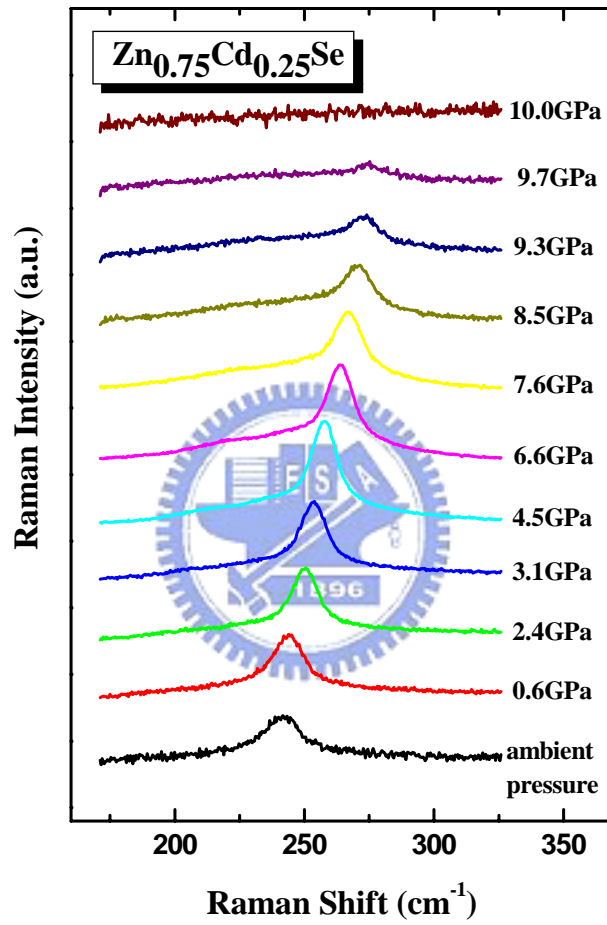Fig. 3.6   Raman spectra frequency of $Zn_{0.86}Cd_{0.14}Se$ at different pressure.

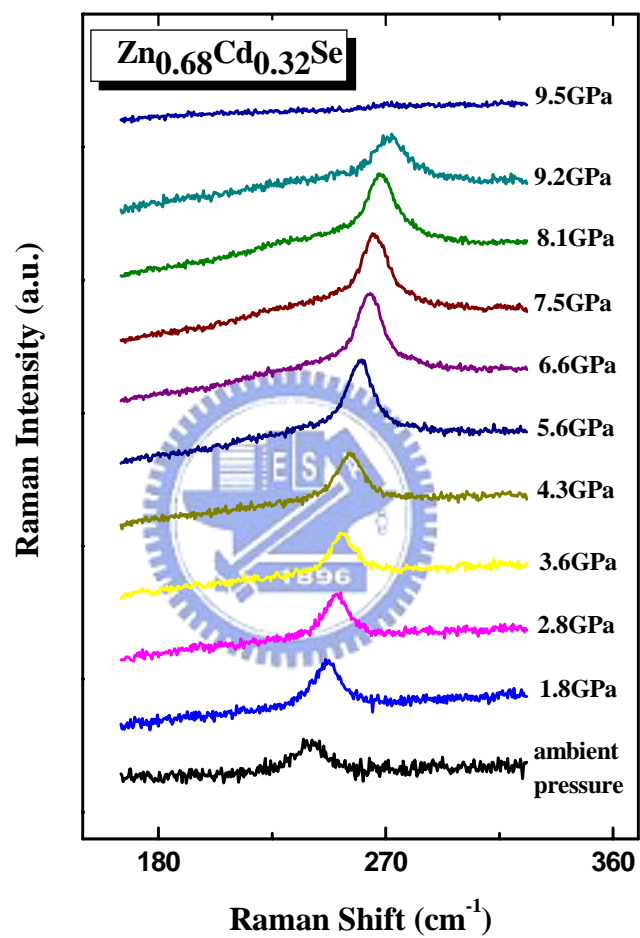Fig. 3.7　Raman spectra frequency of $Zn_{0.75}Cd_{0.25}Se$ at different pressure.

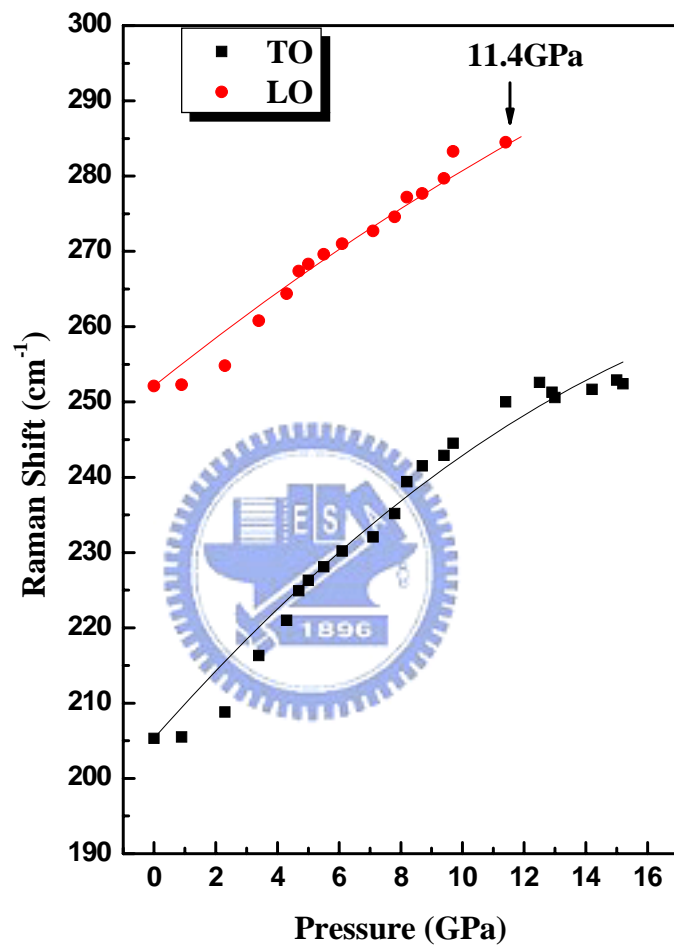Fig. 3.8   Raman spectra $Zn_{0.68}Cd_{0.32}Se$ at different pressure.
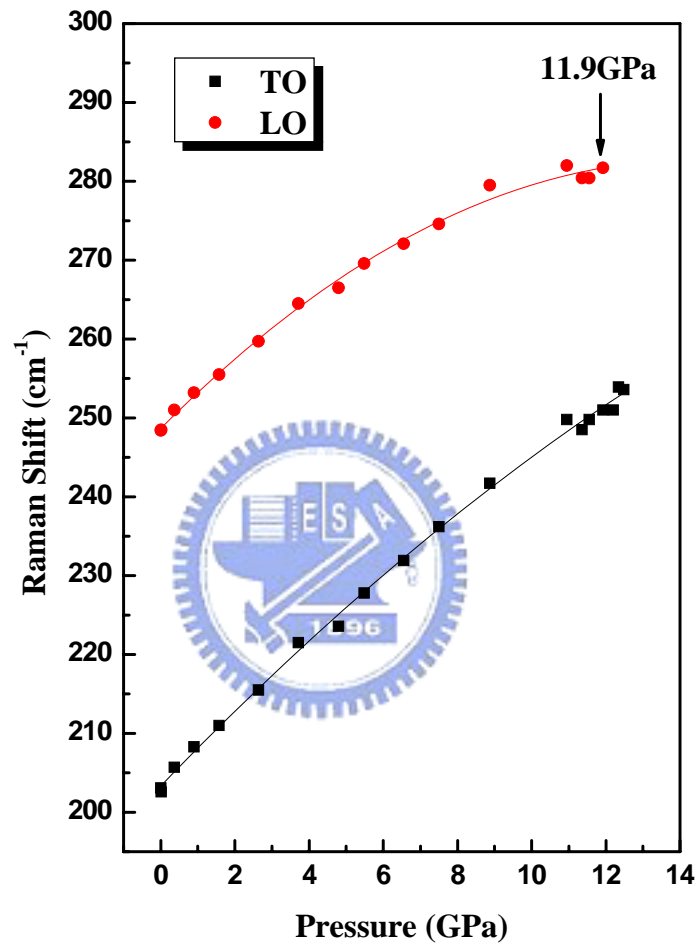
Fig. 3.9   Pressure dependence of LO and TO peaks for ZnSe.

Fig. 3.10　Pressure dependence of LO and TO peaks for $Zn_{0.94}Cd_{0.06}Se$.

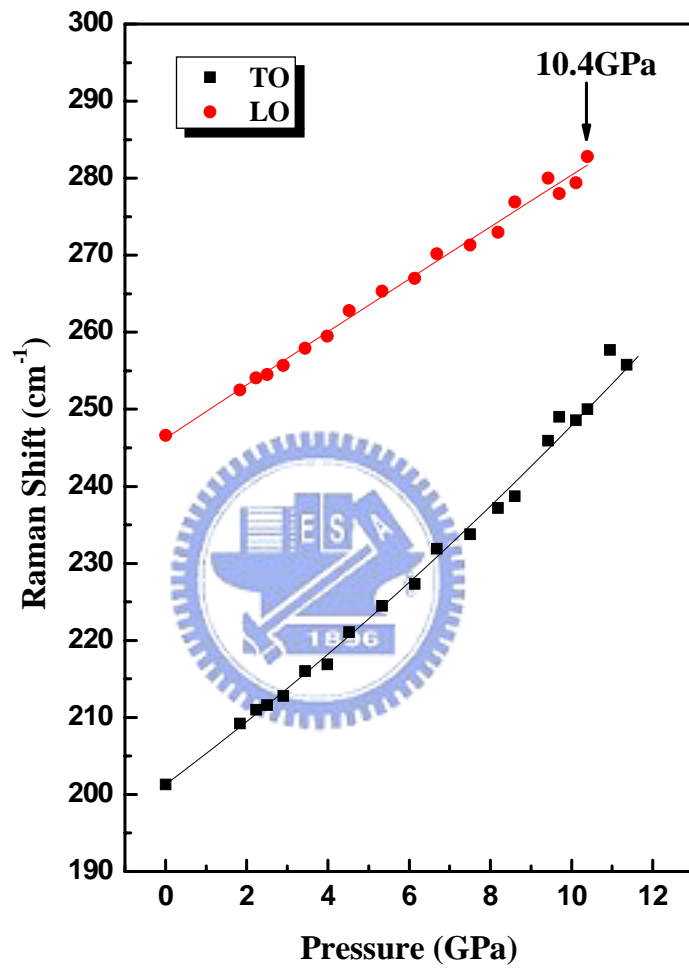Fig. 3.11　Pressure dependence of LO and TO peaks for $Zn_{0.92}Cd_{0.08}Se$.
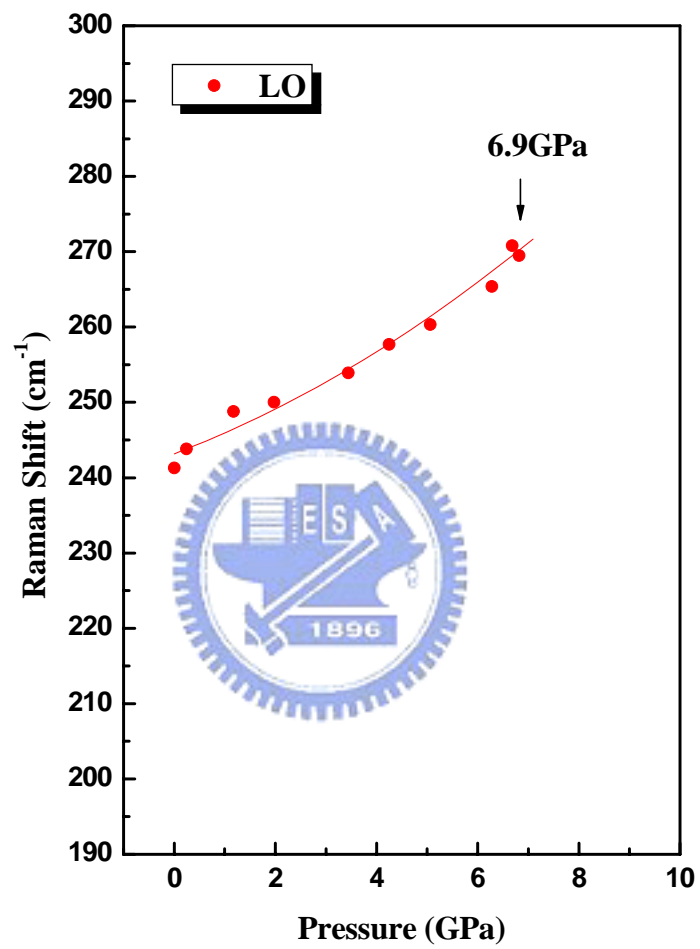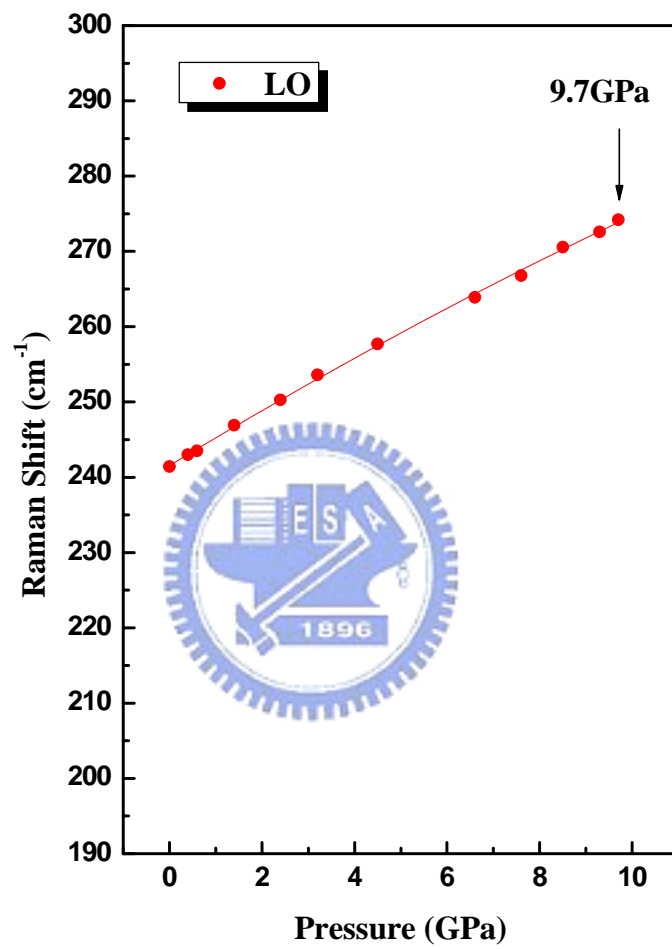
Fig. 3.12　Pressure dependence of LO peak for $Zn_{0.86}Cd_{0.14}Se$.

Fig. 3.13　Pressure dependence of LO peak for $Zn_{0.75}Cd_{0.25}Se$.
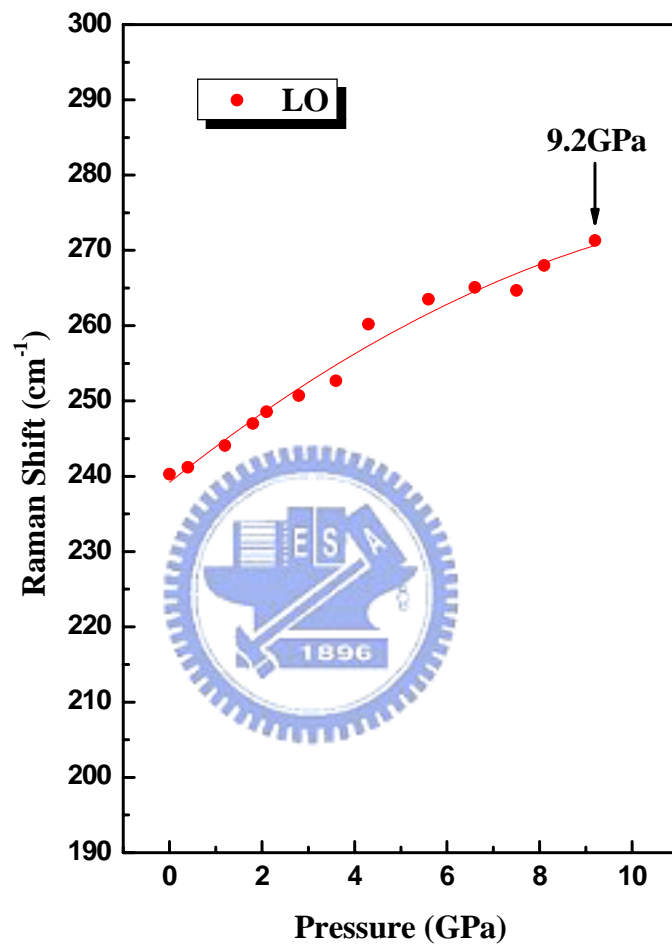
Fig. 3.14   Pressure dependence of LO peak for $Zn_{0.68}Cd_{0.32}Se$.
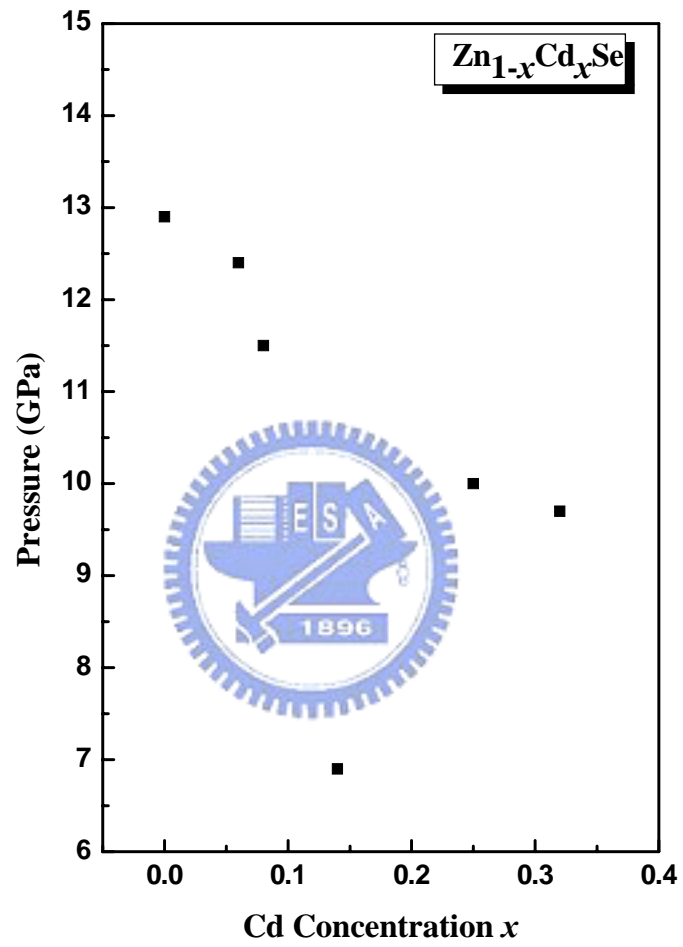
Fig. 3.15　Concentration dependence of transition pressure for $Zn_{1-x}Cd_xSe$

epilayers.

Chapter 4
Conclusion

The pressure-induced structural phase transition of $Zn_{1-x}Cd_xSe$ epilayers was investigated using the micro-Raman scattering experiment. From the Raman scattering experiment, we have measured the frequencies of LO and TO phonons in $Zn_{1-x}Cd_xSe$ epilayers for $x = 0.00, 0.06, 0.08, 0.14, 0.25$, and 0.32 at room temperature and various pressures. Indirect observation of the metallization of semiconductors was proposed. The disappearance of the LO phonon is attributed to the metallization of the $Zn_{1-x}Cd_xSe$ epilayers. The pressure-induced metallization for ZnSe, $Zn_{0.94}Cd_{0.06}Se$, $Zn_{0.92}Cd_{0.08}Se$, $Zn_{0.86}Cd_{0.14}Se$, $Zn_{0.75}Cd_{0.25}Se$, and $Zn_{0.68}Cd_{0.32}Se$ epilayers occurred at 12.9, 12.3, 11.4, 7.1, 10.0, and 9.5 GPa, respectively. The observed reduction in the structural transition pressure of $Zn_{1-x}Cd_xSe$ with Cd concentration implies that the replacement of Zn by Cd results in a decrease in the metallization pressure. This also indicates that the replacement of Zn by Cd results in a softening of the crystal bonding and instability of the crystal structure. The pressure variation of the phonon frequencies and Grünesien parameters of the two optical modes were also calculated.

References

[1]   W. Meredith, G. Horsburgh, G. D. Brownlie, K. A. Prior, B. C. Cavenett, W. Rothwell, and A. J. Dann, J. Cryst. Growth **159**, 103 (1996).

[2]   M. A. Haase, J. Qiu, J. M. Depuydt, and H. Cheng, Appl. Phys. Lett. **59**, 1272 (1991).

[3]   J. Ding, H. Jeon, T. Ishihara, M. Hagerott, and A. V. Nurmikko, H. Luo, N. Samarth, and J. Furdyna, Phys. Rev. Lett. **69**, 1707 (1992).

[4]   S. Ves, K. Strössner, N. E. Christensen, C. K. Kim, and M. Cardona, Solid State Commun. **56**, 479 (1985).

[5]   M. I. McMahon and R. J. Nelmes, J. Phys. Chem. Solids **56**, 485 (1995).

[6]   R. G. Greene, H. Luo, and A. L. Ruoff, J. Phys. Chem. Solids **56**, 521 (1995).

[7]   G. Itkin, G. R. Hearne, E. Sterer, M. P. Pasternak, and W. Potzel, Phys. Rev. B **51**, 3195 (1995).

[8]   C. M. Lin, D. S. Chuu, T. J. Yang, W. C. Chou, J. A. Xu, and E. Huang, Phys. Rev. B **55**, 13641 (1997).

[9]   M. P. Halsall, P. Harmer, P. J. Parbrook, and S. J. Henley, Phys. Rev. B **69**, 235207 (2004).

[10]   C. Pinquier, F. Demangeot, J. Frandon, J. W. Pomeroy, M. Kuball, H. Hubel, N.W. A. van Uden, D. J. Dunstan, O. Briot, B. Maleyre, S. Ruffenach, and B. Gil, Phys. Rev. B **70**, 113202 (2004).

[11]   C. Pinquier, F. Demangeot, J. Frandon, J. C. Chervin, A. Polian, B. Couzinet, P. Munsch, O. Briot, S. Ruffenach, B. Gil, and B. Maleyre, Phys. Rev. B **73**, 115211 (2006).

[12]   J. Bak, U. Venkateswaran, C. L. Mak, R. Sooryakumar, and B. T. Jonker, J.

Phys. Chem. Solids **56**, 563 (1995).

[13]   A. K. Arora, and T. Sakuntala, Phys. Rev. B **52**, 11052 (1995).

[14]   A. K. Arora, E. K. Suh, U. Debska, and A. K. Ramdas, Phys. Rev. B **37**, 2927 (1988).

[15]   J. Xu, J. Yen, Y. Wang, and E. Huang, High Pressure Research **15**, 127 (1996).

[16]   R. A. Forman, G. J. Piermarini, J. D. Barnett, and S. Block, Science **176**, 284 (1972).

[17]   E. Huang, J. Geol. Soc. China **32**, 924 (1992).

[18]   G. J. Piermarini and S. Block, Rev. Sci. Instrum. **46**, 973 (1975).

[19]   A. Chergui, J. Valenta, and J. L. Loison, Semiconductor Science Technology **9**, 2073 (1994).

[20]   J. I. Packove, *Optical Processes in Semiconductors*, Dover, New York (1971).

[21]   R. G. Alonso, E. K. Suh, A. K. Ramdas, N. Samarth, H. Luo, and J. K. Furdyna, Phys. Rev. B **40**, 3720 (1989). I. F. Chang and S. S. Mitra, Phys. Rev. **172**, 924 (1968).

[22]   I. F. Chang and S. S. Mitra, Phys. Rev. **172**, 924 (1968).

[23]   W. Meredith, G. Horsburgh, G. D. Brownlie, K. A. Prior, B. C. Cavenett, W. Rothwell, and A. J. Dann, J. Crystal Growth **159**, 103 (1996).

[24]   J. Camacho, I. Loa, A. Cantarero, K. Syassen, I. Hernández-Calderón, and L. Gonzálz, Phys. Stat. Sol. (b) **235**, 432 (2003).

[25]   W. S. Li, Z. X. Shen, D. Z. Shen, and X. W. Fan, J. Appl. Phys. **84**, 5198 (1998).

[26]   L. K. Vodopyanov, N. N. Melnik, and Yu. G. Sadofev, Semiconductors **33**,

286 (1999).

[27]   M. Cardona and G. Güntherodt, *Light Scattering in Solids IV*, Springer, Berlin (1984).

[28]   O. Madelung, *Semiconductors :Data Handbook*, Springer, Berlin (2004).

[29]   F. Benkabou, H. Aourag, and M. Certier, Mater. Chem. Phys. **66**, 10 (2000).

[30]   S. S. Mitra, O. Brafman, W. B. Daniels, and R. K. Crawford, Phys. Rev. **186**, 942 (1969).

作者簡介

姓名：吳聲嵩

出生日期：**71/02/21**

學歷：國立交通大學顯示工程研究所
　　　私立中原大學電子工程學系
　　　國立陽明高級中學